Fermilab

Doc Number: Beams-doc-7540
Version: 1.0
Category: Note

Radiation Studies for Main Injector Activation Using MARS in a 'Toy Model'

Phil Adamson, Bruce C. Brown, Nikolai Mokhov, and Vitaly Pronskikh
Accelerator Division
Fermi National Accelerator Laboratory *
P.O. Box 500
Batavia, Illinois

9 August 2019

*Operated by Fermi Research Alliance under contract with the U. S. Department of Energy

Contents

Abstract

MARS [1] [2] [3] [4] studies of energy deposition and activation in the Main Injector tunnel are supplemented with studies with a simplified geometry in which the loss of 8 GeV protons are modeled in a cylindrical geometry. We use this to provide a more computer-efficient source for understanding. We build this model to compare with the Main Injector 20-Ton collimators and activation studies of materials placed at the C307 Collimator. Using these studies, we confirm basic activation issues for the Main Injector collimator region while exploring issues with various elements in order to determine which minor elements or isotopes may be important while removing concern about materials for which detailed specification can now be shown to not be of interest. We will explore the activation of steel as measured in special studies, examine activation of minor components of steel and document MARS results for the activation of various compositions of concrete and stainless steel. Results will be compared with some measurements and implications for long term tunnel activation issues will be examined.

1 Introduction

The MARS model which was used for studies to gain approval for the Main Injector Collimators [5] is compute intensive. While we update it for further analysis, we have a more computationally efficient model (Toy Model) of the secondary collimators which matches it well enough to allow us to gain insight into the various physics issues with much better turn-around time on the computers. With this model, we have explored several issues which inform concerns to pursue further.

The study of activation of Steel and Copper in Beams-doc-4046 [6] employed 'tags' of Main Injector Steel, Copper, and Aluminum with an initial goal of discovering what isotopes and thereby what half lifes would be of interest for radiation monitoring in the tunnel. We had already shown [7] that the residual radiation levels in the tunnel could be related to the loss monitor values at nearby loss monitors by assuming a small number of isotope half lives. The tags were in locations on the side (Shielded) of the collimator and on the downstream end above the beam pipe (Unshielded) at a small angle from the interacting beam.

A few surprises such as the significant activation of Antimony (Sb) caused us to continue the MARS efforts in order to better understand what was observed. Meanwhile we also want to explore any long term issues which we might have failed to notice by predicting any long half life isotopes and evaluating their impact on tunnel activities. With this in mind, we will use this model to explore the MARS predictions for the activation studies, explore expected activation issues in the tunnel walls (concrete), beam pipe (316L Stainless Steel and more recently some 2205 Stainless) and other issues which will allow understanding of tunnel activation.

We remark that the results in Beams-doc-4046 were presented as activation rates which were corrected to provide the equilibrium activation to be achieved at a specified loss rate. We will provide such rates from these studies. In getting these equilibrium rates we will choose to first correct our results to a produced activation for a given total loss as if it happened in a time short compared to the half life. These are simply related by the half life (or life time) but we call this out to reduce confusion.

We will introduce various concerns and describe their significance for the radiation issues created by loss of 8 GeV protons. We will then provide detailed results. Some concerns will be addressed separately in appendices where we will also separate out some of the studies.

1.1 Elements in Concrete

In review of the MI tunnel, one can consult Chapter 4 of the Main Injector Technical Design Handbook[8]. The concrete in the Main Injector tunnel arrived in three parts. The floor was poured over 'undisturbed' glacial till (clay). The stairways and nearby features were formed and poured. The bulk of the walls and ceilings were created with precast reinforced concrete. Each of these are likely to have come from separate sources of materials. If we describe concrete as a mixture of Portland cement, sand, and aggregate, we can expect the aggregate to potentially be different for the three tunnel construction types. We explored the content using an x-ray fluorescence spectrometer but the paint on the tunnel wall (TiO_2) limited the signals available on most walls. We did get spectra from the floor and a few places on the walls and conclude that detailed chemical results are likely to be difficult to obtain with high reliability. We choose a different strategy. MARS has a standard concrete description. We will using MARS to determine whether likely differences from that description will impact the expected activation patterns.

The native rock available for creating aggregate in Illinois is mostly limestone (calcium carbonate - $CaCO_3$) and dolomite ($CaMg(CO_3)_2$) or mixtures thereof. Ca experiences very low activation. We will use this Toy Model to explore what we might expect for tunnel activation of Mg with many years of exposure for tunnel walls near the Main Injector collimators. The MARS Build-in ordinary concrete (Table 10) results will be supplemented with Mg samples in the toy model. The fluorescence spectroscopy has limited sensitivity to Mg so a different chemical analysis would be required if this is important.

A result from the fluorescence spectroscopy is that several of the measured spectra show Zirconium (Zr). After some discussion, we conclude that the observed level (somewhat different in spectra from different tunnel locations) is consistent with the natural abundance of Zr (1.3×10^{-4}). Since it is a heavier nucleus than most of the materials in the tunnel, we will ask MARS whether it is likely to be activated to a degree which is of interest.

1.2 Minor Elements and Isotopes in Iron

The activation study reported in Beams-doc-4046 [6] reported observation of Fe-59, Sb-121, and Sb-123. Initial discussions of these results suggested that they are due to neutron capture on Fe-58, Sb-120, and Sb-122. The reported activation is not entirely negligible in the iron sample measurements so we have exerted some effort to understand these results. To better understand, we will also explore other steel compositions and explore what the impact on activation might be.

1.3 Elements in Various Stainless Steels

The 304 stainless steel at the heart of the Main Injector and Recycler collimators is similar to the 316L Stainless in the beam pipes in the tunnel but its activation products are well shielded by steel and marble so it has small impact for the radiation issues for the collimation system with one exception. Some monitoring of the residual radiation has been carried out by measuring at the downstream end of the four collimators where the monitoring point is on the outer surface of the stainless steel vacuum liner. Of additional interest however, we have replaced some of the 316L beam pipe with 2205 (duplex) stainless steel beam pipe in high radiation areas of the Main Injector. This alerted us to be interested in potential activation issues with the many elements in our stainless steel. In particular, the duplex stainless has a significantly higher Molybdenum (Mo) content. Since it is a heavier nucleus, we will explore its activation properties. For completeness, we will also document those properties for other common elements in stainless steel including Cr, Ni, and Mn.

For P, S, and N we will assert that at the known concentration, they do not activate for half life values of interest to our studies.

2 Formulas

In examining the activation with a large range of half life values, we will look at expectations for different time ranges. Let us examine the formulas for production of activation. We will employ notation similar to that in Beams-doc-4046 [6]. In a beam of particles, nuclear interactions produce new isotopes. The number of new nuclei is proportional to the fluence, Φ, measured in particles per unit area (particles-cm^{-2}). In a material with n_S sample atoms, an interaction with cross section σ_I will produce n_I atoms of isotope I in the sample volume.

$$n_I = \Phi n_S \sigma_I. \tag{1}$$

Given a lifetime of τ_I or a half life of $t_{1/2} = \tau_I / \ln 2$, the activity, S (Bq), produced by n_I atoms is

$$S(Bq) = \frac{n_I}{\tau_I} = \frac{n_I \ln 2}{t_{1/2}} = \frac{\Phi n_S \sigma_I}{\tau_I} = \frac{\Phi n_S \sigma_I \ln 2}{t_{1/2}} \tag{2}$$

For these MARS calculations, we calculate the activity in Bq for the sample and use the sample volume and density to convert to specific activity while converting to pCi. For a volume, V, and density ρ we will have n_S/V target atoms per unit volume (cm^3) or $n_T = n_s/\rho V$ atoms per gram. We will want the specific activity per gram of target material

$$S_A(Bq/gm) = \frac{n_I}{V \rho_S \tau_I} = \frac{n_I \ln 2}{V \rho_S t_{1/2}} = \frac{\Phi n_T \sigma_I \ln 2}{V \rho_T t_{1/2}} \tag{3}$$

Substituting for n_T with $\rho_T N_A / A_T$ we have

$$S_A(Bq/gm)(Produced) = \frac{\Phi N_A \sigma_I}{A_T \tau_I} = \frac{\Phi N_A \sigma_I \ln 2}{A_T t_{1/2}} \tag{4}$$

which we will describe as the activity produced by fluence Φ

$$S_A(pCi/gm)(Produced) = \frac{\Phi N_A \sigma_I}{A_T \tau_I 3.7 \times 10^{-2}} = \frac{\Phi N_A \sigma_I \ln 2}{A_T t_{1/2} 3.7 \times 10^{-2}} \tag{5}$$

The particles (mostly hadrons) produced by Φ is proportional to the number of interacting protons, p so let us describe it by $\Phi(p) \times p = \frac{d\Phi}{dp} \times p$ with protons interacting at a rate $\frac{dp}{dt}$ such that $\frac{d\Phi(t)}{dt} = \frac{d\Phi}{dp}\frac{dp}{dt}$ or $\Phi = \frac{d\Phi(t)}{dp} \times p$.

$$S_A(Produced)(Bq/gm) = \frac{N_A \sigma_I}{A_T \tau_I} \frac{d\Phi}{dp} p \tag{6}$$

or

$$S_A(Produced)(pCi/gm) = \frac{N_A \sigma_I}{A_T \tau_I 3.7 \times 10^{-2}} \frac{d\Phi}{dp} p \tag{7}$$

Considering production for time t_1 with a uniform $\frac{dp}{dt}$ and cooldown for time t_c we have the standard activation formula (see Eq. 10 of Beams-doc-4046 or Eq. 3.9 of Barbier [9]) reframed for $\Phi(p)$.

$$S_A(t_c)(Bq/gm)(observed) = \frac{N_A\sigma_I}{A_T}\frac{d\Phi}{dp}\frac{dp}{dt}(1-e^{-t_i/\tau_I})e^{-t_c/\tau_I} = S_A(Produced)\frac{\tau_I}{p}\frac{dp}{dt}(1-e^{-t_i/\tau_I})e^{-t_c/\tau_I} \quad (8)$$

The number of interacting protons is $p = t_i\frac{dp}{dt}$ so $(1/p)\frac{dp}{dt} = 1/t_i$. For these MARS studies, the activation time, t_i, is 30 days and the cooldown time, t_c, is 2 hours. For isotopes with lifetimes $t_i \gg \tau_I$, the decays will match the production (equilibrium) and we again consider Eq. 8 but both decay corrections are now zero if we consider a time while activation is ongoing (no decay after activation). We find that

$$S_A(Bq/gm)(equilibrium) = \frac{N_A\sigma_I}{A_T}\frac{d\Phi}{dp}\frac{dp}{dt} = S_A(Produced)\frac{\tau_I}{p}\frac{dp}{dt} = S_A(Produced)\frac{\tau_I}{t_i} \quad (9)$$

Using Eq. 6 for the Produced Activation, Eq. 8 for Observed Activation after uniform exposure and a period of cooldown or Eq. 9 for the Equilibrium activation for a given isotope I, we can relate these quantities for a given MARS study. More generally, we will wish to have these results normalized to a rate of delivery, ($\frac{dp}{dt}$) or a total number of delivered protons, p.

$$S_A(\frac{(Bq/gm)}{(p/sec)})(equilibrium) = \frac{N_A\sigma_I}{A_T}\frac{d\Phi}{dp} = S_A(Produced)\frac{\tau_I}{p} \quad (10)$$

where for this calculation we can use the $S_A(Produced)$ from our simulation as corrected using Eq. 8. We note that the fluence, $\Phi(p)$ is a property of the shielding configuration between the proton interaction point and the sample. The MARS study will employ as specified beam loss rate, $\frac{dp}{dt}$ which along with the exposure time, t_i and the cooldown time, t_c are required to understand the observed activation. Should we want the total produced activation per proton (related by τ_I to the total number of produced atoms, n_I), we use Eq. 8, correct for decay during excitation and cooldown and divide by $\frac{\tau_I}{p}\frac{dp}{dt} = \frac{\tau_I}{t_i}$.

We can obtain the produced activation per proton as

$$S_A((Bq/gm)/p)(produced) = \frac{1}{\tau_I}S_A((Bq/gm)/(p/sec)(equilibrium) \quad (11)$$

In review, we note that for equilibrium production for a given isotope, the number of protons which contribute to the equilibrium activation is lifetime $\times$ rate: $p = \tau_I\frac{dp}{dt}$.

3 Toy Model Description

3.1 Toy Model Geometry

In the Main Injector collimators, 8 GeV beam impinges on the inside of a stainless steel collimation core. Our activation studies (Beams-doc-4046) have been carried out on the outside of the marble shielding at a large angle from the beam (shielded location) and at a small angle from the beam on the front face of the collimator (unshielded location). The Toy Model has been constructed to simulate this configuration in an calculationally efficient manner.

The Toy Model collimator is a 200 cm long cylinder with a 3.8 cm inner bore radius and a 63.5 cm outer radius. The first 36 cm of the inner bore are tapered from 4.4 cm at the entrance to 3.8 cm. The collimator main body in the model is made of the yoke steel (green), with a stainless steel

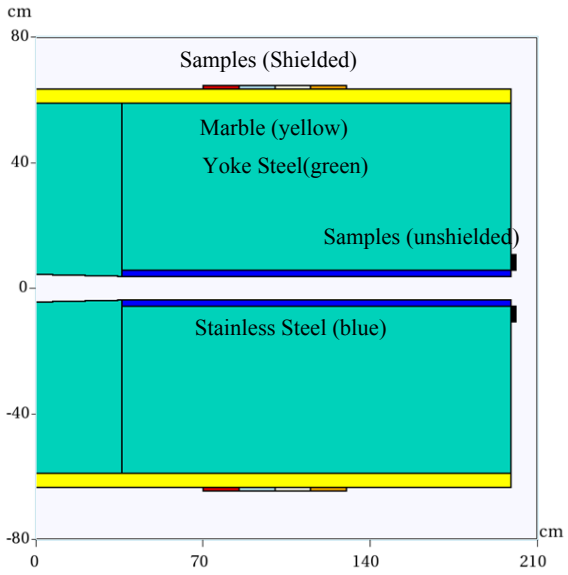

Figure 1: Geometry of Toy Model. Beam enters from the left to strike the liner at the end of the tapered portion. MARS description is in Appendix A

(blue) inner (1.9 cm thickness) and a marble (yellow) outer layer (4.5 cm thickness). The pencil-like proton beam of 1.25E12 p/s is parallel to the cylinder axis. It strikes the inner surface of the bore at the end of the tapered part (30 cm from the entrance to the collimator) on the bottom. The "shielded" samples are 1 cm thick cylinders. They are placed onto the outer surface of the marble layer at large angles ($52.5^o, 45^o, 39^o, and\ 34.25^o$) with respect to the proton beam. The "unshielded" ones - near the exit at the downstream end of the collimator are 0.5 cm thick cylinders stacked at small angles ($\approx$ 50 mRadians).

3.2 Toy Model Execution

For these studies, we employ runs with 1.25×10^{12} protons per second interacting at 36 cm into the collimator at the end of the inner tapered portion of the toy model. Each calculation describes a 30 day activation and a 2 hour cool down period. The results use MARS to calculate the produced isotopes and the decay and (potential) transmutation are calculated using DeTra which is called through MARS. The output describes the activity which has been produced and remains at the end of the 30 days plus 2 hours.

By using DeTra, the isotopes are ordered by the activation at the end of the run. For a sample, the activity is calculated in becquerel (Bq) which is decays per second in the sample. Isotopes are required to have a half life >0.1 h and activities > 1 Bq are reported. The sample volume is noted. Using the sample density and the conversion from becquerel (Bq) to curies (Ci) we examine results for specific activity in pCi/gm[1].

[1] In some of the files of results, the density used for this conversion is the density of Iron. The correction for the actual density of the sample was done in the spreadsheet for each sample.

3.3 Toy Model particle flux and dose distributions

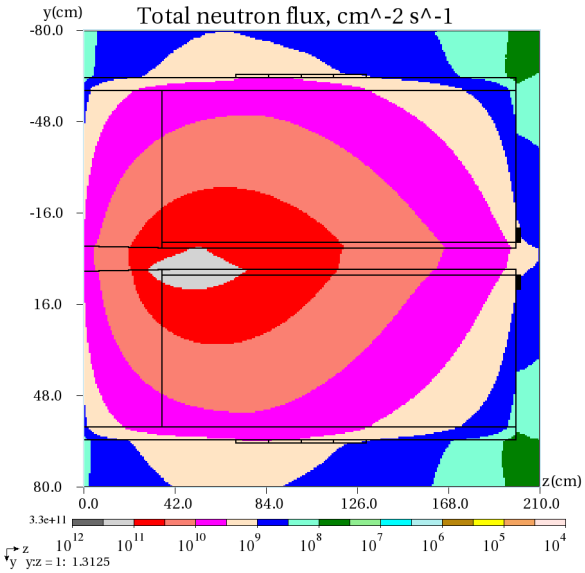

Figure 2: Total neutron flux (0.001 eV $\leq$ E_n $\leq$ 8 GeV) in the Toy Model.

Using elevation views of the Toy Model, we see the distribution of neutrons (Fig. 2), protons (Fig. 3), photons (Fig. 4), and positrons and electrons (Fig. 5). The residual dose after a 1 day cooldown is shown in Fig. 6. To gain insight into the angular distributions, we see the neutrons in a cross section at the interaction point (Fig. 7) and a cm beyond the downstream end of the collimator (Fig. 8).

3.4 Toy Model-2 unshielded particle spectra

Toy Model-2 is the modification of Toy Model in which unshielded samples are represented as four concentric nested rings, with the thicknesses R_{out} - R_{in} = 2.5 cm. The innermost ring has R_{in} = 5.7 cm (radius of the inner bore), and the outermost has R_{out} = 15.7 cm. These samples are then at angles of 42.5, 57.8, 73.1 and 88.3 mRadians. The particle spectra in Figures 9-11 are simulated for the particles crossing the upstream surfaces of each of the rings.

The spectra in Figures 9-11 indicate that while neutrons dominate at low energies, the fluxes of protons and neutrons are comparable at 100 MeV (where inelastic interactions and cascades dominate). However, at the latter energy, proton fluxes in the innermost and outermost rings differ by a factor of 5 (factor of 10 for photons). Therefore, angular differences in production rates can be also significant.

4 Analysis

For uniform activation, the correction for decay during activation is easily expressed. Similarly, the decay after excitation is also easy. This has been described as the standard activation formula as shown in Eq. 8. Dividing by the decay corrections, we obtain the produced activation (Eq. 6). At this point we divide by the number of protons which interacted to provide the activation per proton. Finally, we can multiply by the lifetime to obtain the equilibrium activation per proton per second.

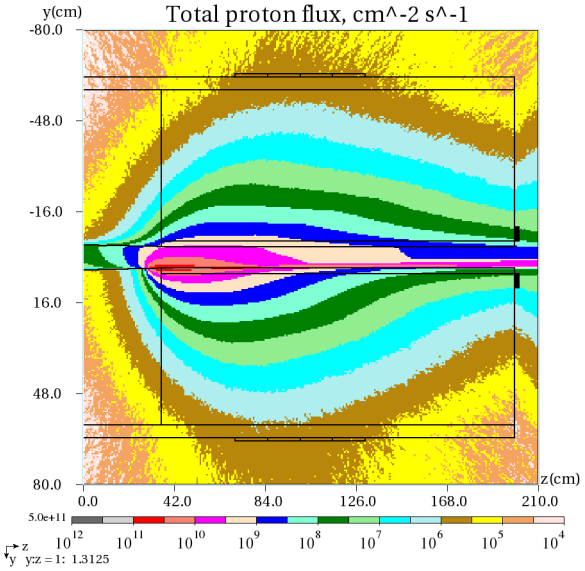

Figure 3: Total proton flux (1 keV $\leq$ E_p $\leq$ 8 GeV) in the Toy Model.

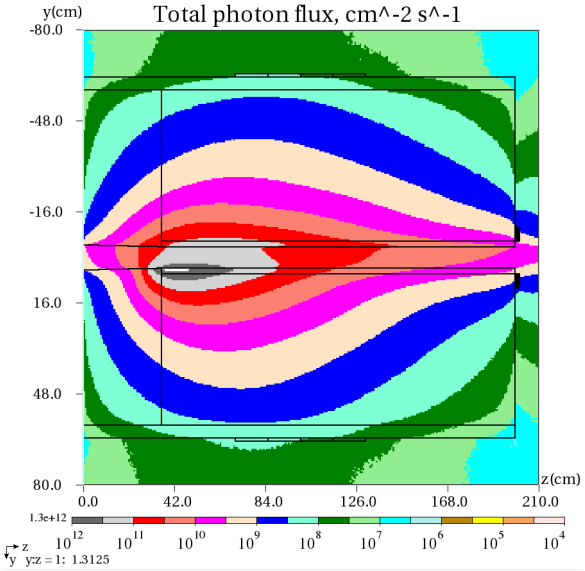

Figure 4: Total photon flux (100 keV $\leq$ E_γ $\leq$ 8 GeV) in the Toy Model.

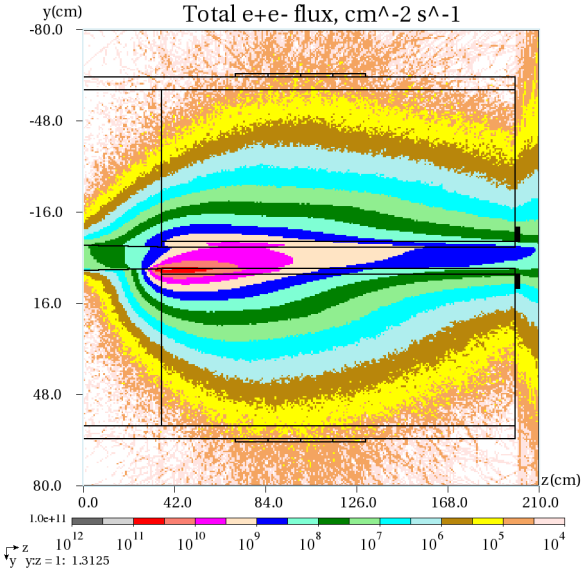

Figure 5: Total positron+electron flux (10 MeV $\leq E_{e^+e^-} \leq$ 8 GeV) in the Toy Model.

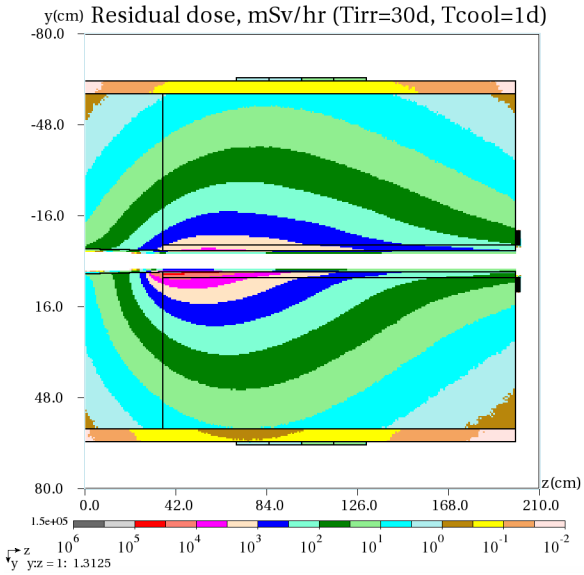

Figure 6: Total residual dose on contact with the Toy Model after irradiation.

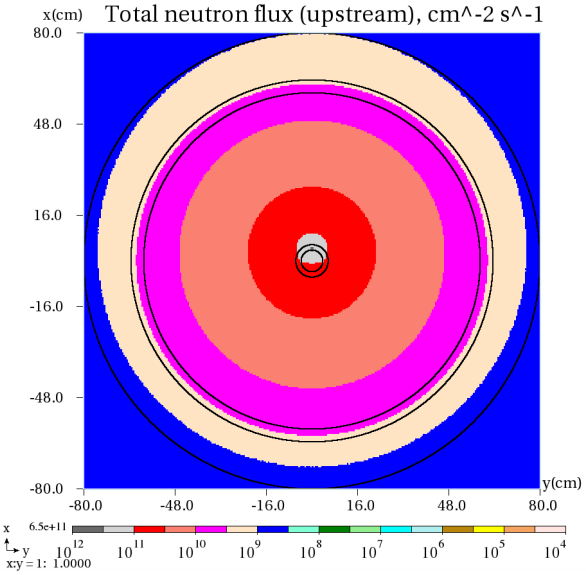

Figure 7: Total neutron flux (0.001 eV $\leq$ E_n $\leq$ 8 GeV) in the Toy Model. XY view at Z=36 cm (beam interaction point).

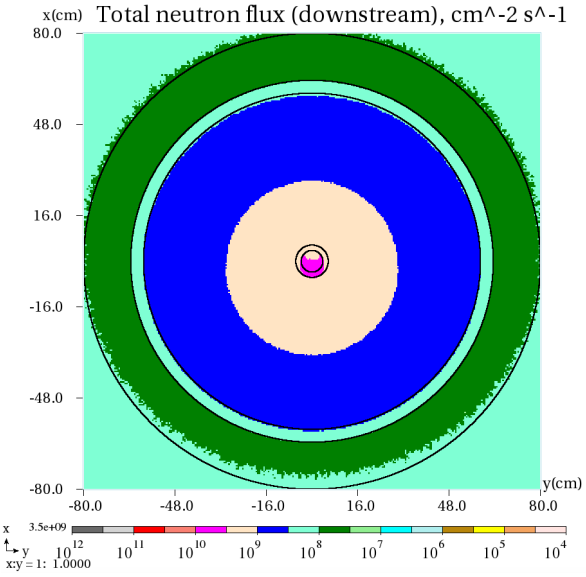

Figure 8: Total neutron flux (0.001 eV $\leq$ E_n $\leq$ 8 GeV) in the Toy Model. XY view at Z=200 cm (downstream end of collimator).

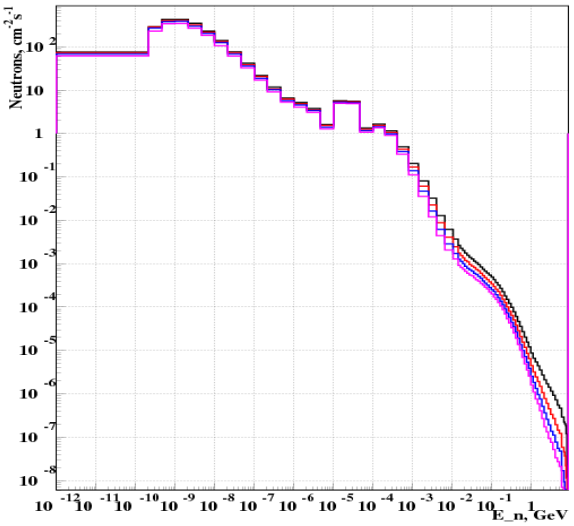

Figure 9: Neutron spectra in Toy Model-2 unshielded sample locations. Black – first (innermost), red – second, blue – third, magenta – fourth (outermost).

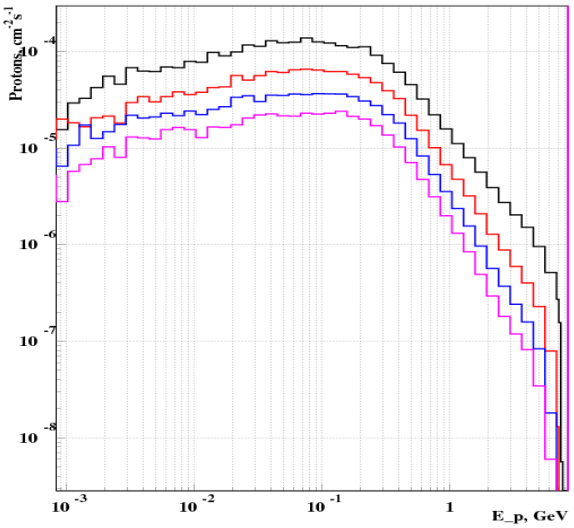

Figure 10: Proton spectra in Toy Model-2 unshielded sample locations. Black – first (innermost), red – second, blue – third, magenta – fourth (outermost).

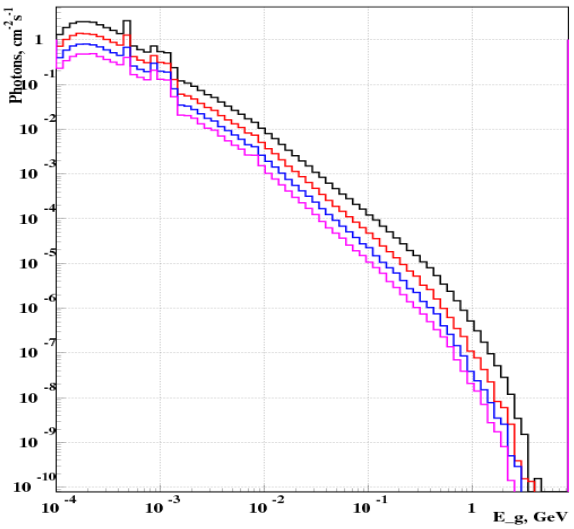

Figure 11: Photon spectra in Toy Model-2 unshielded sample locations. Black – first (innermost), red – second, blue – third, magenta – fourth (outermost).

We discuss some results by comparing the equilibrium activation for the MARS run in pCi/gm without dividing by the protons/sec.

5 Results

This report is based on several MARS runs with various samples. We choose to describe several of the studies in appendices where we review results from one or a few MARS runs. In this section we will describe some of the major topics for which we have conclusions.

A typical MARS result allows the reader to examine the spectrum on cooling in a single graph. We provide that for Concrete in Figure 12

5.1 Typical Activation Levels

When exploring any particular activation issue, the MARS toolset provides many sorts of outputs including activation levels and cool down curves. Our particular situation involving loss of 8 GeV protons in the Main Injector Collimators will be further explored with simulations of that system. This study is more general in that we seek to gain knowledge of the sensitivity of our efforts to many details for which we will decide how thoroughly we will explore to determine the exact configuration of our devices. With that in mind, we will summarize some of the overall activation properties of some interesting materials. Using our 30 Day activation with 2 hour cool down MARS studies, arbitrarily, we will provide the equilibrium activation for the samples in pCi/gm for the specific activation rate of our study. The results in pCi/gm/(p/sec) are available in the analysis spreadsheets. While we occasionally want results for 2 hours of cool down since we can hurry into the tunnel and make measurements then, more typically we want results for days or more with

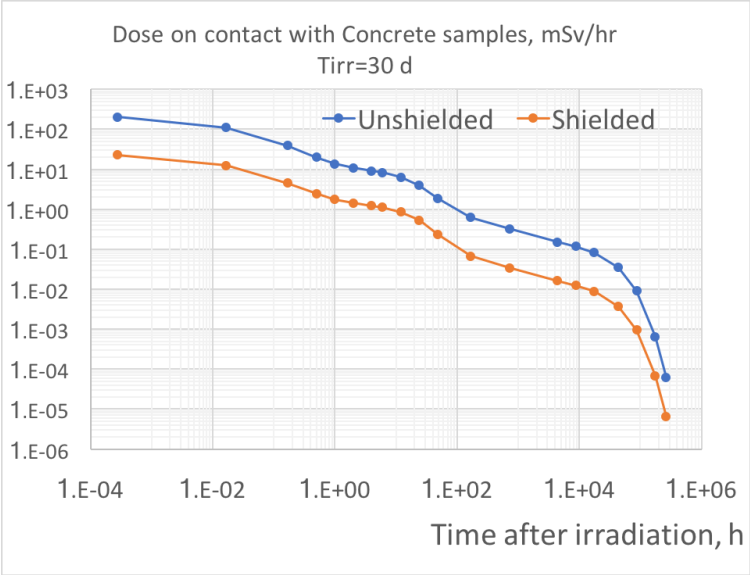

Figure 12: Activation of Concrete shown with logarithmic cooling times.

potential cool down up to 12 weeks (2016 hours or 7.26×10^6 seconds). To explore personnel exposure, we need answers to about 20% and will attempt to arrive at 5% accuracy. We could re-sort the MARS output to provide the equilibrium activation properly ordered. Instead, we will keep the list as sorted by activation after 30 days/2 hrs and sum activation over about 99% of the activation. Some unimportant activation is calculated for long lifetimes. We choose to label half lives longer than 20 years and declare that we will not expect to reach equilibrium for those isotopes.

In Table 1 we have shown the calculated equilibrium activation for our nominal loss rate. The Unshielded location sees a higher energy and more intense flux than the shielded location. The limit of 1 Bq in the sample is for the sample volume at each location but the shielded samples have nearly $\times 50$ more volume. This accounts for the otherwise surprising results that the total number of isotopes with >1 Bq is larger in shielded samples for many of the lighter elements and materials. Despite this volume difference the list of produced isotopes in unshielded samples is longer for chromium and heavier elements. The choice of isotopes to include in the activation sum was not precise. The total activation is nearly unaffected but a careful sorting would result in a different number of isotopes to be included. Frequently isotopes with half lives shorter than 2 hours were included and rarely ones with half life longer than 20 year were also added in but in neither case were they added if a substantial change would be made in the sum. If the reader is particularly interested in this aspect of these results, the spreadsheet results may be of interest (or one can re-sort the MARS outputs) since for several of the samples, one or two isotopes may contribute a large fraction of the activation.

We also would note that the entire exercise is based on the decay rate in Bq. For this reason, the radiological impact of some of the most significant activation products by decay rate are not really that important for energy deposited or biological impact. For example, Fe-55 produces only keV gammas (or do you say x-rays) and they are not readily detected by the Geiger counters we employ for radiation monitoring.

Table 1: MARS Results on Summed Equilibrium Activation at 1.25×10^{12} protons interacting per second.

Material	Isotopes >1 Bq	Isotopes in sum	Activation pCi/gm
Unshielded			
MI Steel	75	33(inc ^{3}H)	2.68E+07
SS 316L	152	49(inc ^{3}H)	2.98E+07
Concrete	43	33	6.13E+06
Copper (uns6)	71	53	3.31E+08
Magnesium	9	9	1.32E+07
Calcium	27	22	3.83E+07
Titanium	28	46	1.35E+07
Chromium	53	49	2.27E+07
Manganese	56	42	1.82E+08
Iron	59	46	2.24E+07
Nickel	68	41	2.79E+07
Zirconium	151	116	9.90E+07
Molybdenum	178	61(inc ^{3}H)	1.01E+08
Shielded			
MI Steel	83	31(inc ^{3}H)	5.79E+06
SS 316L	153	48 (arb)	1.36E+07
Concrete	52	40	7.36E+05
Copper (shi10)	66	45	5.66E+07
Magnesium	9	9	1.96E+06
Calcium	31	20	7.70E+05
Titanium	42	28	1.84E+06
Chromium	49	49	4.17E+06
Manganese	53	40	1.48E+08
Iron	56	44	2.71E+06
Nickel	62	24	2.76E+06
Zirconium	116	63	3.32E+06
Molybdenum	140	50	9.26E+07

5.2 Manganese Activation

Since the studies which correlated loss to activation ("Measuring Correlations Between Beam Loss and Residual Radiation in the Fermilab Main Injector") [7], we have known that Mn-56 (half life of 2.5789 hours) was an important contributor to the radiation for early access to the accelerator tunnel. By examining the activation of steel samples and pure Fe as reported in Appendix E we gain an appreciation for what is involved. Two facts stand out when examining those results:

- The activation ratio for Mn-56 for unshielded to shielded is small (0.783 - 1.292) for the steel samples whereas it is large (8.77) for the Fe sample. This small ratio is not typical of the products of spallation reactions. For the measurements in Beams-doc-4046 [6] the ratio of Unshielded/Shielded as 4.545 which is also very low among the measured samples.
- For Mn-56, the ratio of Fe/(steel) is very small for all three steel materials for both the shielded and unshielded samples.

Together, these suggested that much of the Mn-56 activation was likely to be due to neutron capture. Since each of these samples contain some Mn which is nearly 100% Mn-55, we will examine the analysis results for consistency with that speculation.

Table 2: MARS results on Mn-56 Production. MARS results are corrected for decays to provide the produced activation of the target material. Corrected column accounts for the weight fraction of Mn in the sample.

Target	Wt Frac of Mn	pCi/gm/p	pCi/gm/p
Material		MARS	Corrected
Unshielded			
MI Steel	0.0052	1.07E-10	2.05E-08
SS316	0.02	2.90E-10	1.45E-08
CAST Iron	0.0018	4.20E-11	2.34E-08
Mn	1.00	1.31E-08	1.31E-08
Shielded			
MI Steel	0.0052	1.06E-10	2.04E-08
SS316	0.02	3.70E-10	1.85E-08
CAST Iron	0.0018	3.26E-11	1.81E-08
Mn	1.00	1.17E-08	1.17E-08

We note that the production of Mn-56 in iron is much smaller but not negligible. MARS predicts that 2.36E-12 pCi/g/p is produced in the shielded location while 2.30E-11 pCi/g/p is produced in the unshielded location. The ratio of Unshielded/Shielded for Fe is 8.78 while the Fe/MI Steel is 0.0248 for shielded but 0.216 for shielded. These are suggestive of a spallation reaction to produce Mn-56 in Iron. It also is in the appropriate direction to explain the difference in the unshielded results for CAST Iron.

When we explore the results of fitting Bar-coded residual radiation measurements to half-life weighted loss monitor (BLM) measurements, we had been concerned that the fraction attributed to Mn-56 was more variable than we had expected. Now we conclude that the different materials should have different Mn-56 production. We successfully describe the residual radiation at about the 20% level by assuming that dominant isotopes other than Mn-56 are Mn-54 and Mn-52. Their production from various materials appears to be more 'ordinary.'

5.3 Production of Fe-59 and Fe-55

The observation of Fe-59 in the MI-Steel sample [6] was assumed to be due to neutron capture on Fe-58. MARS upgrades have allowed this to be explored in these studies. The measurements failed to observe Fe-59 in the unshielded results (but this is likely due to limited effort as this study was terminated). The ratio of Unshielded/Shielded for Fe-59 is consistent with being dominated by neutron capture (smaller ratios).

MARS predicts significant activation of Fe-55 but the resulting 5.9 keV x-rays have limited penetration and low energy such as to produce little radio-logical impact. MARS results will show up in spreadsheets but we will not discuss them further. The HPGe detector used for the activation studies in Beams-doc-4046 does not provide a useful measurement for such low energies.

5.4 Compare MARS Toy Model Activation to Measurements for MI Steel

The MARS simulations have provided guidance for comparisons of the activation in the Main Injector Collimator region. The Toy Model provides a similar geometry to understand important issues but we do not expect a complete match to the measured results reported in Beams-doc-4046-v3 [6]. At this point we will show that we are agreeing with the measurements at the level we might have expected. Plots shown in Figures 13 and 14 show that various isotopes have similar rates for Measured and MARS with Measured/MARS = 3.489 for the unshielded samples suggesting that the Toy Model geometry is too long (162 cm in Model vs. 127 cm in 20-T Collimators) between the interaction point and the samples whereas the Measured/MARS = 0.553 for the Shielded samples would indicate that there is not enough shielding in the model for those samples (due to different longitudinal position (detection angle) and less marble). Table 3 allows the reader to examine this information for many produced isotopes.

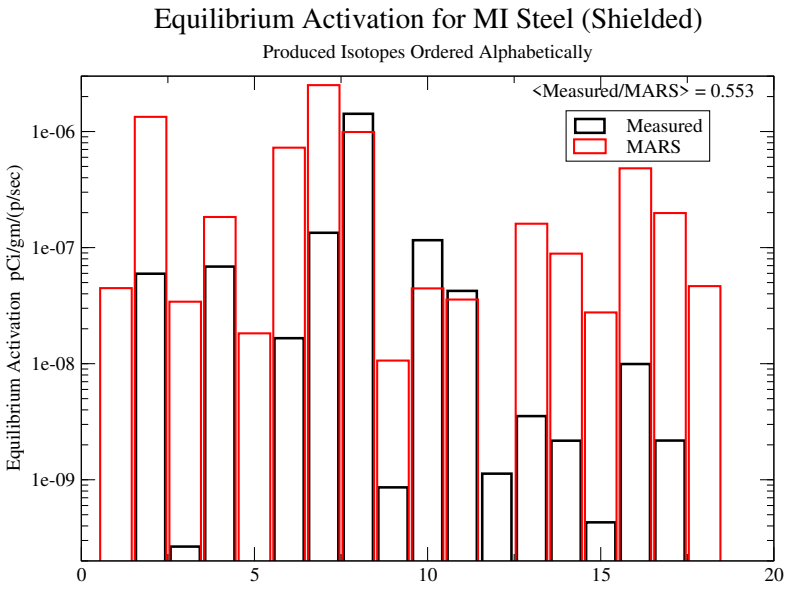

Figure 13: Equilibrium Activation of MI Steel at Shielded Location. Isotopes are shown in order provided in Table 3.

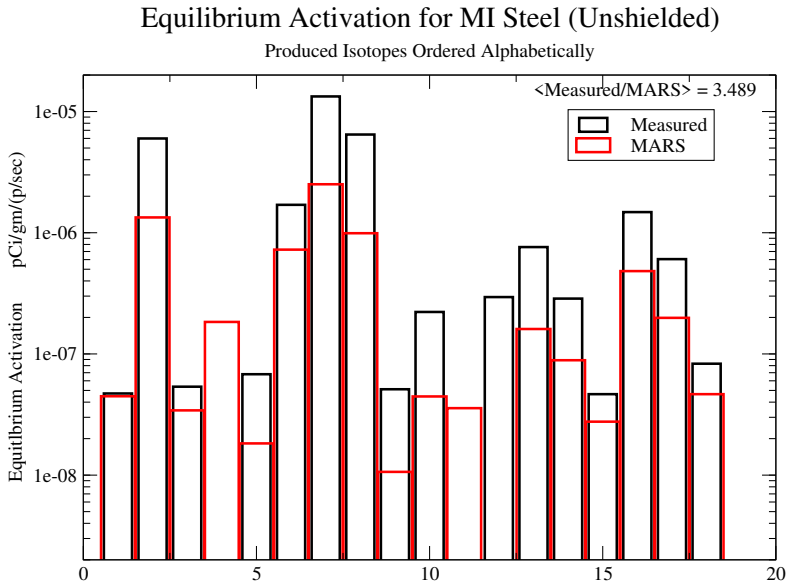

Figure 14: Equilibrium Activation of MI Steel at Unshielded Location. Isotopes are shown in order provided in Table 3.

Table 3: Activation of Main Injector Steel from Measurement and MARS

	Element	Half Life	Measured		MARS		Measured/MARS	
		Days	pCi/gm/(p/sec)		pCi/gm/(p/sec)			
			Shielded	Unshielded	Shielded	Unshielded	Shi	Unshi
1	Cr-48	0.89833		4.715E-08	3.198E-09	4.474E-08		1.054
2	Cr-51	27.7	5.960E-08	5.994E-06	1.689E-07	1.338E-06	0.353	4.481
3	Fe-52	0.344792	2.657E-10	5.365E-08	3.280E-09	3.422E-08	0.081	1.568
4	Fe-59	44.5	6.866E-08		6.299E-08	1.837E-07	1.090	
5	K-43	0.9292		6.801E-08	7.783E-10	1.826E-08		3.724
6	Mn-52	5.591	1.658E-08	1.700E-06	8.587E-08	7.256E-07	0.193	2.343
7	Mn-54	312.2	1.341E-07	1.332E-05	4.214E-07	2.510E-06	0.318	5.305
8	Mn-56	0.1074	1.420E-06	6.455E-06	9.848E-07	9.90E-07	1.442	6.520
9	Na-24	0.62329	8.607E-10	5.109E-08	6.053E-10	1.064E-08	1.422	4.803
10	Sb-122	2.7	1.159E-07	2.218E-07	1.265E-07	4.454E-08	0.916	4.981
11	Sb-124	60.2	4.240E-08		9.555E-08	3.568E-08	0.444	
12	Sc-44m	2.44	1.129E-09	2.945E-07				
13	Sc-46	83.83	3.534E-09	7.611E-07	9.060E-09	1.605E-07	0.390	4.741
14	Sc-47	3.341	2.171E-09	2.859E-07	5.895E-09	8.868E-08	0.368	3.224
15	Sc-48	1.82	4.296E-10	4.655E-08	1.934E-09	2.762E-08	0.222	1.685
16	V-48	15.98	9.934E-09	1.480E-06	3.627E-08	4.821E-07	0.274	3.070
17	Sc-44	0.1654	2.177E-09	6.054E-07	9.502E-09	1.985E-07	0.229	3.050
18	K-42	0.515		8.309E-08	1.568E-09	4.656E-08		1.785

5.5 MARS Toy Model Results for Copper with Comparison to Measurements

For a Toy Model run to study copper samples, we uses four shielded and four unshielded samples. We gain an understanding of the sensitivity to the geometry specific to the four stacked unshielded samples and the different angles/absorption depths for the shielded samples. We also have measurements of these samples reported in Beams-doc-4046 and we compare Meas/MARS. The sample ratio comparisons for the most important 10 isotopes are shown in Figures 15 and 16. A sense of the expected relative activation for the four shielded locations is provided by the flux plots in Figures 2 thru 4. The results on the four shielded samples are consistent with expectations from the flux plots. Table 4 documents the Measured and MARS results for isotopes for which Beams-doc-4046 has results.

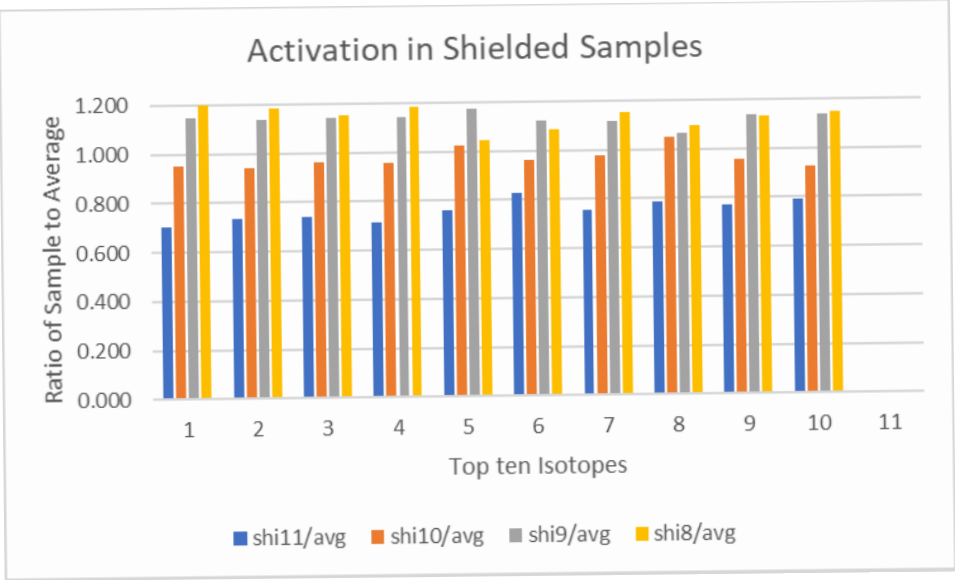

Figure 15: Ratio of sample activation to mean of samples for shielded Cu samples. These samples differ in angle but also in absorption depth. Isotopes are shown in order employed in Table 4.

6 Conclusion

As outlined above, our purpose was to draw conclusions about the required specification detail for materials in the region of the Main Injector Collimation System. As we developed this information, we found that we have also a more general picture of the activation properties of a variety of materials and elements. Among conclusions we draw from there studies:

- For activation of concrete, we will wish to suggest some care with regard to the production of Na-24 but that has only a 15 hour half life so it has little impact when planning tunnel activities. For Na-22, the activation is not large while aggregate of pure dolomite (mineral) would add 50% to 100% to the production of Na-22 so some care may be required for very careful activation studies. The contribution of zirconium will be negligible.

- The activation of Mn-56 is consistent with being dominated by neutron capture on Mn-55 for many materials in our tunnel.

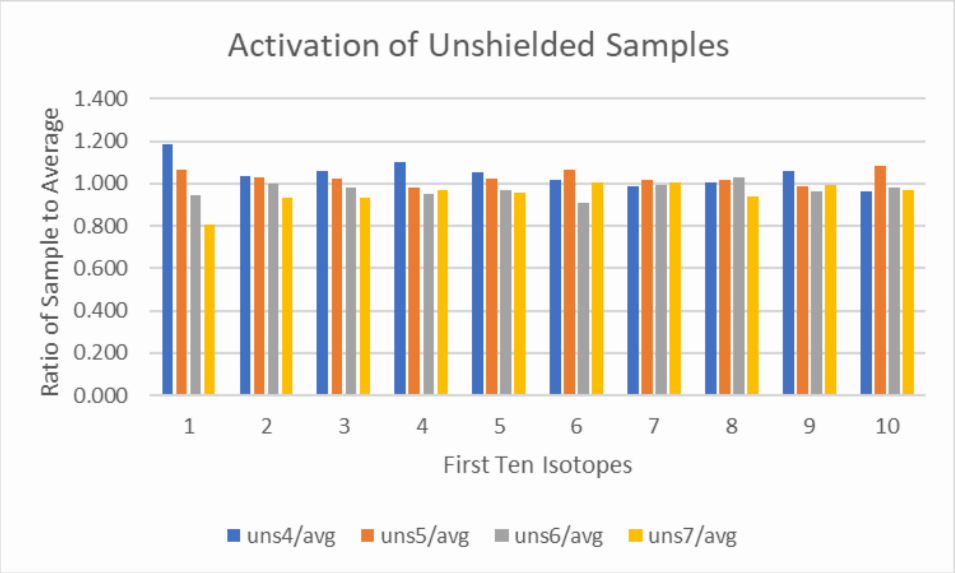

Figure 16: Ratio of sample activation to mean of samples for unshielded Cu samples. These samples span a range of angles near the beam. Isotopes are shown in order employed in Table 4.

Table 4: Activation of Copper from Measurement and MARS.
Average Meas/MARS is 0.401 for Shielded (shi8) and 3.4949 for Unshielded (uns7)

	Element	Half Life	Measured		MARS		Measured/MARS	
		Days	pCi/gm/(p/sec)		pCi/gm/(p/sec)			
			Shielded	Unshielded	Shielded	Unshielded	Shi	Unshi
1	Co-55	0.7304		8.15E-08	2.592E-09	4.069E-08		2.002
2	Co-56	77.233	4.812E-09	9.74E-07	1.691E-08	1.834E-07	0.285	5.308
3	Co-57	271.74	2.52E-08	2.83E-06	8.244E-08	6.919E-07	0.305	4.092
4	Co-58	70.86	4.048E-08	4.61E-06	1.360E-07	9.280E-07	0.298	4.970
5	Co-60	1925.8	2.758E-08		8.843E-08	4.936E-07	0.312	
6	Cr-51	27.7	4.261E-09		1.247E-08	2.571E-07	0.342	
7	Cu-61	0.139		4.19E-06	1.761E-07	1.002E-06		4.181
8	Cu-64	0.5291	5.471E-05	1.04E-04	5.061E-05	4.774E-05	1.081	2.172
9	Fe-59	44.5	2.909E-09		7.115E-09	4.580E-08	0.409	
10	K-43	0.9292		4.39E-08	8.042E-11	7.949E-09		5.520
11	Mn-52	5.591	1.816E-09	3.36E-07	6.259E-09	1.223E-07	0.290	2.748
12	Mn-54	312.2	1.024E-08		2.890E-08	3.581E-07	0.354	
13	Mn-56	0.1074		5.75E-07	7.773E-09	8.677E-08		6.628
14	Na-24	0.62329		1.28E-08		2.929E-09		4.379
15	Ni-57	1.4833		7.77E-08	2.686E-09	3.240E-08		2.399
16	Sc-44m	2.44		7.90E-08				
17	Sc-47	3.341		4.65E-08	8.372E-10	3.388E-08		1.373
18	Sc-48	1.82		2.74E-08	2.680E-10	1.004E-08		2.727
19	V-48	15.98	1.114E-09	1.73E-07	3.375E-09	1.003E-07	0.330	1.729
20	Sc-44	0.1654		1.16E-07	9.562E-10	5.272E-08		2.198

- We observe that the equilibrium activation of various materials is different, confirming the understanding that we can avoid high activation with some materials. Molybdenum and Manganese are more highly activated but typical concentrations are not high. While Copper is also more highly activated, the produced isotopes for Copper typically have shorter half lives.

We have employed the activation for a 30 day exposure and 2 hour cooldown which we converted to a total produced activation and an equilibrium activation. While this is a convenient analysis tool, we did not find that the use of produced activation provided new insight.

For the measurements in Beams-doc-4046, we found two classes for the Ratio Uns/Shi which seemed to correlate with spallation (high ratio) and neutron activation (low ratio). In searching for this correlation in the MARS Toy Model results, we found that the geometry explored failed to reproduce the very large ratios. We attribute that to the specifics of the study geometry and find that looking at Uns/Shi ratios in this study was sometimes suggestive of production mechanisms but not sufficient to provide useful guidance.

A presentation on the Toy Model at SATIF12 [10] used older MARS code and a different tactic for the comparison. In addition to the improved agreement due to detailed specification of the sample isotopes, we find that comparing equilibrium activation explicitly allows better matching to the exposure history of the measurements.

With the study of sensitivities in this work, we believe we are ready to resume MARS studies of the activation of the Main Injector Collimation region.

A Typical MARS Geometry Description

A typical set of MARS Input Files:

File: GEOM.INP

```
Detector Solenoid geometry
!OPT

collim1 2 0 1 0.0 0.0 36.0 3.8 5.7 163.
collim2 2 0 2 0.0 0.0 36.0 5.7 59. 163.
collim3 2 0 3 0.0 0.0 0.0 59. 63.5 199.
taper1  4 0 2 0.0 0.0 0.0 4.4 59. 3.8 59. 36.
uns1    2 0 4 0.0 0.0 199.  5.7 10.7 0.5
uns2    2 0 5 0.0 0.0 199.5 5.7 10.7 0.5
uns3    2 0 6 0.0 0.0 200.0 5.7 10.7 0.5
uns4    2 0 7 0.0 0.0 200.5 5.7 10.7 0.5
shi1    2 0 8  0.0 0.0 70.  63.5 64.5 15.0
shi2    2 0 9 0.0 0.0 85.  63.5 64.5 15.0
shi3    2 0 10 0.0 0.0 100. 63.5 64.5 15.0
shi4    2 0 11 0.0 0.0 115. 63.5 64.5 15.0
TR1     0.0 0.0 0.0 0.0 90.0 0.0
stop
```

---

fILE: MATER.INP

```
 m1516 BCB with MCNP6 neutron libraries   11/28/17

1 'STST'
2 'YOKE'
3 'MRBL'
4 'STEEL' 7.85 9
 5.5845E+01   2.6000E+01 0.987484
 1.2011E+01   6.0000E+00 0.000033
 5.4938E+01   2.5000E+01 0.0052
 3.0974E+01   1.5000E+01 0.00051
 3.2066E+01   1.6000E+01 0.00006
 2.8085E+01   1.4000E+01 0.0036
 2.6982E+01   1.3000E+01 0.00276
 1.4007E+01   7.0000E+00 0.000023
 1.2176E+02   5.1000E+01 0.00033
5 'Fe-58' 7.874 1
 58.00000 26.00000 1.000
6 'SB'
7 'ZR'
8 'STEEL' 7.85 9
 5.5845E+01   2.6000E+01 0.987484
```

```
 1.2011E+01   6.0000E+00 0.000033
 5.4938E+01   2.5000E+01 0.0052
 3.0974E+01   1.5000E+01 0.00051
 3.2066E+01   1.6000E+01 0.00006
 2.8085E+01   1.4000E+01 0.0036
 2.6982E+01   1.3000E+01 0.00276
 1.4007E+01   7.0000E+00 0.000023
 1.2176E+02   5.1000E+01 0.00033
9 'Fe-58' 7.874 1
 58.00000 26.00000 1.000
10 'SB'
11 'ZR'
```

B Simplifications for Bateman Equations for Main Injector Radiation

The measurements of activation and residual radiation in the Main Injector tunnel such as those reported in Beams-doc-4046[6] involve activation created by 8 GeV protons with activation times up to decades but measurement after activation following 2 hours or more of cooldown. Only a few materials contain nuclei heavier than iron which limits the decay chains of interest. The total loss at any location is much less than 1×10^{21} protons. We will demonstrate that this can be discussed while discarding most terms in the Bateman Equation with no non-linear terms which would involve striking nuclei produced in the activation process. We will discuss this using the presentation of the Bateman Equations from the DeTra documentation[11]. We will copy this directly from Section 2 of that document.

Decay and transmutation of nuclides can be expressed as

$$\frac{dN_i}{dt} = S_i + \sum_j b_{ji}\lambda_j N_j(t) + \sum_j g_{ji}\sigma_j\phi N_j(t) - \lambda_i N_i(t) - \sigma_i\phi N_i(t) \quad (12)$$

where

- N_i is the abundance of nuclide i,
- S_i is the external production rate of nuclide i,
- b_{ji} is the branching ratio of the decay of nuclide j to nuclide i,
- λ_i is the decay constant of nuclide i,
- g_{ji} is the fraction of absorptions in nuclide j leading to nuclide i,
- σ_i is the spectrum averaged absorption cross section of nuclide i, and
- ϕ is the transmutating flux.

We note that

- The first term on the right is the source term. It is any external production rate of nuclides i.e. it does not depend on any of the abundances N. Below we divide the source term in two components - one is due to fission and the other due to accelerator production.
- The second term describes the build-up rate of the nuclide i due to decay of other nuclides, N_j.
- The third term describes the transmutation production rate of nuclide i from other nuclides, N_j. This term includes both the transmutation of unstable isotopes and activation of the stable ones. Note that, even though the accelerator production of the source term above could also be called transmutation or activation, we have reserved the word transmutation for this reaction only.
- The fourth term gives the decay rate of nuclide i, and the last term defines the depletion of the nuclide i due to its transmutation.

In the solution of Eq. 12 we assume that all the quantities, except N, above are constant i.e. do not depend on time. The assumption is usually well satisfied.

As prescribed by Aarnio, we use the first term to describe the activation produced by loss of 8 GeV protons. There will be no fission in the materials we need to consider. In Beams-doc-4046, we considered two isotopes which decay to isotopes which were found in our measurements and conclude that K-42 is not from decay of Ar-42 and Sc-44 is not from decay of Ti-44 based on measurements with different exposure/cooldown times. We conclude that the second term can be eliminated from our considerations. In similar fashion, we can dismiss the third term since the production rate is insufficient to produce sufficient target nuclides, N_j. Finally, the fifth term can be neglected by the same rate considerations.

With the remaining first and fourth terms in this expression, we conclude that the analysis of activation when the beam exposure time is well-measured can be analyzed using the time-weighting

procedure described in Beams-doc-4046 (and Beams-doc-3980 [12]).

C Examination of Linearity of Activation with Beam Delivered

We also wish to explore any non-linear buildup of activation in our situation. We examine Equation 1. In a beam of particles, nuclear interactions produce new isotopes. The number of new nuclei is proportional to the fluence, Φ, measured in particles per unit area (particles-cm^{-2}). In a material with n_T target atoms per unit volume, an interaction with cross section σ_I will produce n_I atoms per unit volume of isotope I

$$n_I = \Phi n_T \sigma_I. \tag{13}$$

$$\frac{n_I}{n_T} = \Phi \sigma_I. \tag{14}$$

The fraction n_I/n_T will remain small compared to 1 provided the fluence Φ does not exceed a limit set by relevant cross sections, σ. We study losses of 1.25×10^{12} protons/second. This leads to 3.95×10^{19} protons for a year of continuous operations. If these would be lost on an area of 1 mm x 1 mm the fluence would be 3.95×10^{21}. For $\frac{n_I}{n_T} = 0.01$ would require $\sigma = 2.53^{-24}$ cm^2 (2.53 barns) whereas the cross sections of interest are at most many millibarns. As the protons produce a shower of hadrons, the peak number of particles will increase by a factor of up to 10 for 8 GeV showers but they will spread such that the fluence in particles per cm^2 will hardly grow. We argue that calculations of this activation will remain linear in the total proton loss for all issues in our list of concerns. Note that extending the time frame to 10 years will increase the total fluence but then many of the produced isotopes will have decayed. The most significant isotope in our study is Mn-54 with a half-life of 312 days.

D Activation of Natural Ca and Ca-40

Calcium is an important component of concrete and we employ marble ($CaCO_2$) for shielding the secondary collimators in the Main Injector Collimation System. In light of the special activation properties of Ca-40 due to the nuclear shell model feature that it is a 'magic' (closed shell) nucleus, we have taken the opportunity presented by the Toy Model to explore the special nature of Ca-40 compared with natural Ca. The isotopic abundance of natural Ca is shown in Table 14. In determining how to present activation studies, we have chosen this comparison to develop presentation methods for other parts of this study. As discussed in the Section on Formulas, we provide formulas for produced activation and equilibrium activation production and relate them to the activation calculated for 30 Days of activation and 2 hours of cooldown with an interaction rate of 1.25×10^{12} protons/second. To compare with measurements or other studies, we will get produced activation per interacting proton and equilibrium activation per interacting protons per second.

We have explored equilibrium activation in Beams-doc-3980 [12] and Beams-doc-4046 [6] but here we have the results for 30 Days of activation and 2 hours of cool down so we have decided to compare these various representations of the calculated results. In Figure 17 we have plotted the 30 Day/ 2 hr activation with the isotopes in the order of decreasing activation for each sample as sorted by DeTra. We then also plot the produced activation and the equilibrium activation for that same calculation. We noted that the short half life produced activities can be quite large and for very long half lives the equilibrium activation would be very large so we have marked the points on the equilibrium curve with solid green points for the half lives longer than 20 years while we

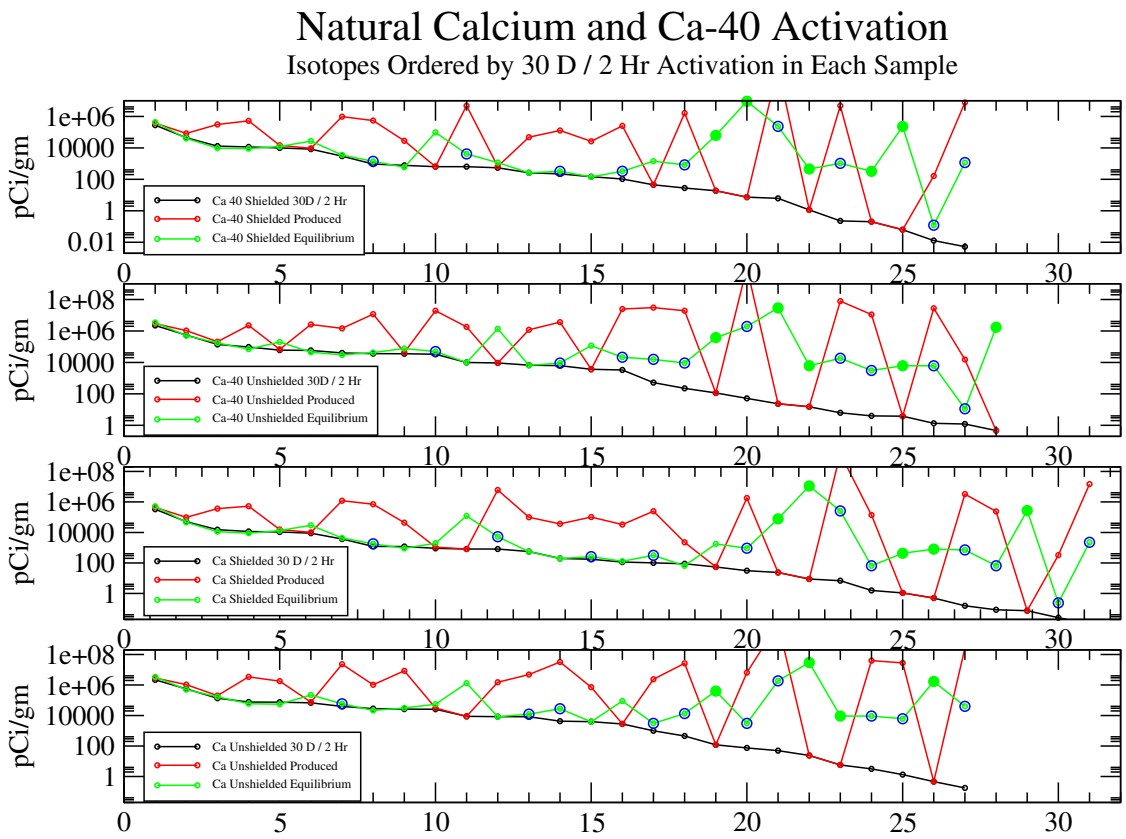

Figure 17: Produced activation in Ca-40 and natural Ca for Shielded and Unshielded locations. Activation after 30 Days of beam on and 2 hours of cooling (black lines and circles) is compared with activation produced by the interacting protons in that run (red lines and circles) and with the equilibrium activation produced at that proton loss rate ((green lines and circles). To clarify the lifetime effects, the equilibrium points for half life values longer than 20 years are shown with solid green circles while those with half life values less than 2 hours are shown with open blue circles.

use open blue circles to identify the equilibrium values for isotopes with half life values less than 2 hours (The list includes ones down to 0.1 hr).

Since the equilibrium activation for Shielded and Unshielded locations are proportional to the proton loss rate, Table 5 and Table 6 provide the equilibrium activation for this study and the equilibrium activation per proton per second. These tables are ordered with the activity from the Ca-shi sample 30 Day / 2 Hr study.

The results and analysis of these samples are available in the spreadsheet Analysis_Concrete_Feb2019.xlsx where the samples with Ca-40 are labeled ca20 (for 20 neutrons and 20 protons).

When we look at the Ratio Table (Table 7) we are forced to realize that some of the potential interesting differences between natural Ca and Ca-40 will have to be explored with higher statistics. We have the σ (standard deviation) for the ratios which are calculated as the root-sum-squares of the errors in each activation and find that the error is too large to draw interesting conclusions. Obviously if the ratio Ca-20/Ca is larger than 1, we must be limited by statistical errors. When the ratio is smaller than 1, we need to look at the RMS error and we see that for no unshielded isotope is there a significantly larger production in the Ca sample. For the shielded samples, we

Table 5: Equilibrium Activation of Ca and Ca-40 – Shielded

				Shielded Ca		Shielded Ca-40	
Element	Z	A	HalfLife	Equilibrium Activation		Equilibrium Activation	
			sec	pCi/gm	pCi/gm/(p/sec)	pCi/gm	pCi/gm/(p/sec)
Ar	18	37	3.03E+06	5.19E+05	4.15E-07	4.34E+05	3.47E-07
P	15	32	1.23E+06	4.63E+04	3.70E-08	4.00E+04	3.20E-08
K	19	43	8.03E+04	1.13E+04	9.02E-09	9.62E+03	7.69E-09
K	19	42	4.45E+04	9.00E+03	7.20E-09	8.99E+03	7.19E-09
P	15	33	2.19E+06	1.32E+04	1.06E-08	1.23E+04	9.84E-09
S	16	35	7.56E+06	2.94E+04	2.35E-08	2.72E+04	2.18E-08
Si	14	31	9.44E+03	4.36E+03	3.49E-09	3.54E+03	2.83E-09
Ar	18	41	6.58E+03	1.81E+03	1.45E-09	1.39E+03	1.11E-09
Na	11	24	5.39E+04	9.13E+02	7.30E-10	5.87E+02	4.70E-10
Be	4	7	4.60E+06	1.96E+03	1.57E-09	1.17E+03	9.39E-10
H	1	3	3.89E+08	1.23E+05	9.85E-08	9.64E+04	7.71E-08
Cl	17	38	2.23E+03	5.27E+03	4.22E-09	4.14E+03	3.31E-09
Sc	21	44	1.43E+04	5.51E+02	4.41E-10	1.44E+02	1.15E-10
Sc	21	43	1.40E+04	1.96E+02	1.57E-10	2.60E+02	2.08E-10
F	9	18	6.59E+03	2.61E+02	2.09E-10	3.26E+02	2.61E-10
S	16	38	1.02E+04	1.30E+02	1.04E-10		
Cl	17	39	3.34E+03	3.17E+02	2.53E-10	3.26E+02	2.61E-10
Mg	12	28	7.53E+04	6.52E+01	5.22E-11		
Na	11	22	8.21E+07	1.76E+03	1.41E-09	1.43E+03	1.15E-09
K	19	44	1.33E+03	9.27E+02	7.42E-10	8.32E+02	6.65E-10
Ar	18	39	8.49E+09	7.77E+04	6.22E-08	6.20E+04	4.96E-08
Ca	20	41	3.22E+12	1.11E+07	8.85E-06	9.21E+06	7.37E-06
K	19	38	4.58E+02	2.56E+05	2.05E-07	2.32E+05	1.85E-07
C	6	11	1.22E+03	6.52E+01	5.22E-11		
Ar	18	42	1.04E+09	4.36E+02	3.49E-10	4.57E+02	3.65E-10
Si	14	32	4.17E+09	8.13E+02	6.50E-10	3.26E+02	2.61E-10
Mg	12	27	5.67E+02	7.17E+02	5.74E-10	1.04E+03	8.35E-10
Ar	18	44	7.12E+02	6.52E+01	5.22E-11		
Cl	17	36	9.50E+12	2.72E+05	2.18E-07	2.31E+05	1.85E-07
Cl	17	34m	1.92E+03	2.41E-01	1.93E-13	1.21E-01	9.65E-14
Al	13	29	3.94E+02	2.25E+03	1.80E-09	1.17E+03	9.39E-10

Table 6: Equilibrium Activation of Ca and Ca-40 – Unshielded

				Unshielded Ca		Unshielded Ca-40	
Element	Z	A	HalfLife	Equilibrium Activation		Equilibrium Activation	
			sec	pCi/gm	pCi/gm/(p/sec)	pCi/gm	pCi/gm/(p/sec)
Ar	18	37	3.03E+06	3.40E+06	2.72E-06	3.45E+06	2.76E-06
P	15	32	1.23E+06	5.05E+05	4.04E-07	4.97E+05	3.98E-07
K	19	43	8.03E+04	5.54E+04	4.43E-08	7.02E+04	5.62E-08
K	19	42	4.45E+04	5.93E+04	4.74E-08	4.47E+04	3.58E-08
P	15	33	2.19E+06	1.69E+05	1.36E-07	1.74E+05	1.39E-07
S	16	35	7.56E+06	2.22E+05	1.77E-07	1.99E+05	1.60E-07
Si	14	31	9.44E+03	3.08E+04	2.46E-08	4.28E+04	3.42E-08
Ar	18	41	6.58E+03	1.23E+04	9.85E-09	9.16E+03	7.33E-09
Na	11	24	5.39E+04	2.15E+04	1.72E-08	3.05E+04	2.44E-08
Be	4	7	4.60E+06	5.54E+04	4.43E-08	7.64E+04	6.11E-08
H	1	3	3.89E+08	1.32E+06	1.06E-06	1.38E+06	1.10E-06
Cl	17	38	2.23E+03	2.77E+04	2.22E-08	2.14E+04	1.71E-08
Sc	21	44	1.43E+04	8.33E+03	6.67E-09	6.54E+03	5.23E-09
Sc	21	43	1.40E+04	3.90E+03	3.12E-09	9.80E+03	7.84E-09
F	9	18	6.59E+03	5.85E+04	4.68E-08	4.89E+04	3.91E-08
S	16	38	1.02E+04				
Cl	17	39	3.34E+03	3.08E+03	2.46E-09		
Mg	12	28	7.53E+04				
Na	11	22	8.21E+07	8.93E+04	7.14E-08	1.17E+05	9.36E-08
K	19	44	1.33E+03	1.35E+04	1.08E-08	1.56E+04	1.24E-08
Ar	18	39	8.49E+09	3.97E+05	3.17E-07	3.78E+05	3.02E-07
Ca	20	41	3.22E+12	3.00E+07	2.40E-05	2.91E+07	2.33E-05
K	19	38	4.58E+02	1.87E+06	1.50E-06	1.94E+06	1.55E-06
C	6	11	1.22E+03	3.08E+03	2.46E-09	9.16E+03	7.33E-09
Ar	18	42	1.04E+09			6.11E+03	4.89E-09
Si	14	32	4.17E+09	9.23E+03	7.39E-09	6.11E+03	4.89E-09
Mg	12	27	5.67E+02	6.16E+03	4.93E-09	6.11E+03	4.89E-09
Ar	18	44	7.12E+02			3.05E+03	2.44E-09
Cl	17	36	9.50E+12	1.70E+06	1.36E-06	1.71E+06	1.37E-06
Cl	17	34m	1.92E+03			1.13E+01	9.04E-12
Al	13	29	3.94E+02	4.00E+04	3.20E-08		
N	7	13	5.98E+02	9.23E+03	7.39E-09	1.83E+04	1.47E-08

Table 7: Activation Ratio of Ca-40/Natural Ca

Element	Z	A	Shielded	σ	Unshielded	σ
Ar	18	37	0.835711427	0.019590378	1.015286456	0.043269619
P	15	32	0.865260494	0.057160137	0.983974388	0.109091963
K	19	43	0.85235126	0.110222173	1.267781778	0.30670135
K	19	42	0.999445538	0.096296458	0.754205899	0.341441102
P	15	33	0.929568489	0.103568808	1.026991349	0.190049992
S	16	35	0.925560457	0.071494469	0.899492028	0.188275921
Si	14	31	0.812189308	0.181102752	1.389482424	0.408982581
Ar	18	41	0.76869496	0.218022456	0.743994688	0.756263672
Na	11	24	0.643073795	0.43944213	1.417542743	0.519764199
Be	4	7	0.599972235	0.314954261	1.378064231	0.320793584
H	1	3	0.783065674	0.038665736	1.046219894	0.070338053
Cl	17	38	0.785110731	0.17499904	0.771812138	0.514820267
Sc	21	44	0.261406676	0.784150472	0.784271397	1.223948392
Sc	21	43	1.325668363	0.581851063	2.510831708	0.79824397
F	9	18	1.249518617		0.835382718	
S	16	38	small			
Cl	17	39	1.030069498			
Mg	12	28	small			
Na	11	22	0.814821774		1.310011964	
K	19	44	0.897333907		1.148617835	
Ar	18	39	0.797134169		0.951756311	
Ca	20	41	0.833292574		0.969894709	
K	19	38	0.905385649		1.038875314	
C	6	11	small		2.977177031	
Ar	18	42	1.046496913			
Si	14	32	0.401355603	0.532929412	0.661499198	0.907767685
Mg	12	27	1.454608853		0.992190498	
Ar	18	44	small		large?	
Cl	17	36	0.850375273		1.002754098	
Cl	17	34m				
Al	13	29				
N	7	13			1.98398702	

see for Ar-37, P-32, K-43 there are statistically significant excess production in the Ca samples and some others show deviations which might indicate an interesting excess but overall, these are the significant isotopes for Ca excess. If we sum the equilibrium activation (using the isotope order of the 30 Day/2 Hr activation) and compare Ca to Ca-40 we find that there is essentially no excess for the unshielded (forward angle) samples. For the shielded (large angle) samples, the Ar-37 is 67% of the activation for both shielded and unshielded and the shielded Ca/Ca-40 ratio is 1.20 for that isotope. Comparing the running sums we find that for the shielded samples, Ca/Ca-40 remains at 1.18 - 1.20 for all sums down to the first very long lived (>20 yr) halflife.[2]

In reviewing this study of Ca and Ca-40, we conclude that emphasizing the study of equilibrium activation is adequate. Using the results from MARS/DeTra for 30 days of activation and 2 hr of cooldown and exploring half life values from 2 hours to 20 years is entirely adequate for the Main Injector activation considerations.

We would now like to quantify the reputation of Ca for low activation. We will compare it to various other materials we have studied in Table 8.

E Toy Model Study with Various Steel Targets

A high statistics study of activation was carried out using a set of four steel varieties as targets. Included were Natural Fe, Main Injector Steel, Cast Iron, and 316 Stainless Steel. The composition used for these materials is shown in Table 12. As in other studies reported in this document, a beam of 1.25×10^{12} protons/sec struck the Toy Model collimator for 30 days after which a cool down of 2 hours was imposed. MARS results were processed with DeTra to provide isotopes produced which were sorted by activity. The files of results were then explored in Excel (file:Analysis_Steels_Oct2018.xlsx). The activation ratios were explored for Unshielded/Shielded for each material. In addition, the activity for each isotope in the unshielded and shielded targets was compared to the production in the natural Fe sample.

F Toy Model Study for Activation of Various Stainless Steel

Stainless steel is a critical component of accelerators and since we employ it for beam pipes, beam loss will almost always activate some stainless steel. We have replaced some 316L stainless pipe with 2205 duplex stainless in a high radiation area near Collimator C301. To acquire some understanding of potential activation issues for these materials, we have toy model runs with samples in both the shielded and unshielded locations for Fe, 316L, chromium (Cr), manganese (Mn), nickel (Ni), and molybdenum (Mo). In Section 5.2 we show results on the activation of manganese. Let us here examine the activation of all of these materials to explore what concerns we should have about how much care in specification of materials is required for the tunnel activation studies. Additionally, we should see what understanding will be helpful in selecting materials for future accelerator components.

Using Toy Model results for the various components of stainless steel, we can simulate the activation of 304, 316, and 2205 alloys. We separately simulated a sample of 316. We find that the results have no surprises. For some produced isotopes like Mn-56, the 2205 is predicted to achieve a lower activation while for many isotopes it 2205/316 is 1.448 so we conclude that use of 2205

[2]When studying the measured activation for Beams-doc-4046, Vernon Cupps noted the possibility of 'Secular Equilibrium' for observing K-42 and Sc-44. After comparing activation with various exposure times, we concluded that we were not seeing Ar-42 $\rightarrow$ K-42 nor Ti-44 $\rightarrow$ Sc-44. These studies are consistent with that for Ca. One can also look for this in the other samples.

Table 8: Comparison of Equilibrium Activation of Various Samples

Element	Z	A	HalfLife	Sample	Activity	Activity
			sec		pCi/gm	pCi/gm/(p/sec)
				Shielded		
Ar	18	37	3.03E+06	Ca	5.19E+05	4.15E-07
P	15	32	1.23E+06	Ca	4.63E+04	3.70E-08
Na	11	24	5.39E+04	Concrete	2.85E+05	2.28E-07
Ar	18	37	3.03E+06	Concrete	7.25E+04	5.80E-08
Si	14	31	9.44E+03	Concrete	4.15E+04	3.32E-08
K	19	42	4.45E+04	Concrete	1.65E+04	1.32E-08
Be	4	7	4.60E+06	Concrete	2.84E+04	2.27E-08
Cu	29	64	4.57E+04	Copper	6.326E+07	5.061E-05
Cu	29	61	1.20E+04	Copper	2.202E+05	1.761E-07
Co	27	58	6.12E+06	Copper	1.700E+05	1.360E-07
Mn	25	56	9.28E+03	MI Steel	1.23E+06	9.85E-07
Mn	25	52	4.83E+05	MI Steel	1.07E+05	8.59E-08
Mn	25	54	2.70E+07	MI Steel	5.27E+05	4.21E-07
				Unshielded		
Ar	18	37	3.03E+06	Ca	3.40E+06	2.72E-06
P	15	32	1.23E+06	Ca	5.05E+05	4.04E-07
Na	11	24	5.39E+04	Concrete	1.01E+06	8.08E-07
Ar	18	37	3.03E+06	Concrete	7.38E+05	5.90E-07
Be	4	7	4.60E+06	Concrete	6.02E+05	4.81E-07
Cu	29	64	4.57E+04	Copper	5.96E+07	4.77E-05
Cu	29	61	1.20E+04	Copper	1.25E+06	1.00E-06
Co	27	58	6.12E+06	Copper	1.16E+06	9.28E-07
Mn	25	56	9.28E+03	MI Steel	1.24E+06	9.90E-07
Mn	25	52	4.83E+05	MI Steel	9.07E+05	7.26E-07
Mn	25	54	2.70E+07	MI Steel	3.14E+06	2.51E-06

alloy should not be restricted due to activation concerns. For those unfamiliar with 2205, we note that is is not suitable for beam pipe through magnets due to its magnetic properties.

G Toy Model Study For Concrete

Studies with samples of concrete in both shielded and unshielded locations were supplemented with samples of Ca, Mg and Zr. Table 10 shows the MARS built-in concrete composition. As discussed in Section 1.1, we have not determined the relative amount of Ca which might be replaced with Mg when the aggregate includes some Dolomite. In spreadsheet Analysis_Concrete_Feb2019.xlsx, we have included the results for comparing concrete with Ca and Mg. In the worksheet:Analysis, we explore the activation of 15.1% of Ca or 15.1% of Mg (the weight fraction of Mg in Dolomite and/or the reduction of Ca) The results are available in the spreadsheet. We choose to look instead at the most significant contributions to the activity in concrete. For both shielded and unshielded concrete samples, the highest activation (sorted by 30 day activation/ 2 hour cooldown) is Na-24 followed by Ar-37.

For Na-24, in the shielded (unshielded) sample the contribution from Ca is only 4.85×10^{-4} (3.23×10^{-3}) and the Mg contribution is x300 (x74) larger however, that Mg contribution is only 14.5% (24%) of the Na-24 in concrete. The Ar-37 in the concrete comes largely from the Ca and no Na-24 is produced in Mg. For shielded concrete, the next two activated isotopes are Si-31 and K-42 where the Ca contribution is modest (or small) and there is no Mg contribution. For the unshielded concrete, the next isotope on the list is Be-7 for which the contribution of either Ca or Mg is very small and Si-31 is next on that list and again Mg would not contribute. Nearby on the list is F-18 where for the unshielded sample, Mg would be quite significant but we declare it not very interesting due to the 1.83 hour half life. We also note that Na-22 falls further down the list with this ordering but would be much higher if ranked by equilibrium activation. For Na-22, the activation from Mg would roughly double the Concrete for shielded samples and provide about 50% more for the unshielded. This might be of interest for very careful activation studies. In looking through all the MARS/DeTra output, only Mg-27 with a half life of 567 seconds shows a very high production on Mg which would be interesting only for pure dolomite in the concrete and for very early observation after excitation.

The Toy Model study of zirconium (Zr) included shielded and unshielded samples. We expected and found that the list of isotopes with activation greater than 1 Bq in the sample was long with 151 isotopes in unshielded zirconium and 116 in the shielded sample. The zirconium equilibrium activation is higher than than concrete with a sum of 3.87×10^{6} pCi/gm for shielded (1.0×10^{8} pCi/gm for unshielded) even when including a few very long half life isotopes which will not reach equilibrium. We compare this with the same total equilibrium activation of shielded concrete (2.54×10^{6} pCi/gm) or unshielded concrete (1.28×10^{7} pCi/gm) and we see that at a weight fraction of 1.3×10^{-4} of zirconium in typical materials on the earth's surface, the contribution of zirconium to our activation studies can be ignored.

H Tables of Selected Material and Nuclear Properties

The reader can find here various items which define the properties of the materials which we study with the Toy Model.

The Wikipedia articles on steels provides most of its information with regard to the EN specification of stainless steel whereas most specifications at Fermilab employ the ASTM designation. Let us have the correlation conveniently available by providing Table 9 here. See

```
https://en.wikipedia.org/wiki/Stainless_steel
    or
https://en.wikipedia.org/wiki/Steel_grades
```

for a source)

Table 9: Stainless Steel Designations

EN	ASTM or SAE
1.4301	304
1.4306	304L
1.4311	304NL
1.4948	304H
1.4401	316
1.4436	316
1.4404	316L
1.4406	316LN
1.4462	2205

Table 10: MARS15 Built-in Ordinary Concrete (density = 2.35 g/cm^3)

Element	Weight Fraction
H	0.006
C	0.03
O	0.50
Na	0.01
Al	0.03
Si	0.2
K	0.01
Ca	0.2
Fe	0.014

References

[1] N. V. Mokhov. The MARS Code System User's Guide. FN 628, Fermilab, April 1995.

[2] N.V. Mokhov, P. Aarnio, Yu. Eidelman, K. Gudima, A. Konobeev, V. Pronskikh, I. Rakhno, S. Striganov, and I. Tropin. MARS15 Code Developments Driven by the Intensity Frontier Needs. *Prog. Nucl. Sci. Technol.*, 4:496–501, 2014. Also FERMILAB-CONF-12-635-APC, 2014.

[3] *MARS15*. URL https://mars.fnal.gov.

[4] Nikolai V. Mokhov and Catherine C. James. The MARS Code System User's Guide Version 15(2016). 2017.

Table 11: Isotopic Content of Iron (from Wikipedia)

Isotope	Abundance
	mole fraction
Fe-54	0.05845
Fe-56	0.91754
Fe-57	0.02119
Fe-58	0.00282

Table 12: Composition (weight fraction) of some common steels. We acknowledge that the specification of most stainless steel and other common steels define a range of elemental content. We will do some calculations with these results so we choose a description which specifies a definite content and will explore whether the differences allowed will become of interest. X-ray fluorescence measurement of Duplex Stainless 2205 beam pipe at MI301 was carried out on 1/22/2015.

Material	Natural Fe	Main Inj Steel	Cast Iron	316 SS	304 SS	2205 SS
Source		Measured	MARS	MARS	MARS	Measured
Fe	1	0.9875	0.9347	0.655	0.695	0.682
Mn	0	0.0052	0.0018	0.02	0.02	0.00736
Cr	0	0	0	0.17	0.19	0.217
Ni	0	0	0	0.12	0	0.0549
Mo	0	0	0	0.025	0	0.0362
Cu	0	0	0.002	0	0	0.00199
Sb	0	0.00033	0	0	0	0
P	0	0.00051	0	0	0	0
S	0	0.00006	0	0	0	0
Si	0	0.0036	0.025	0.01	0	0
N	0	0.000023	0	0	0	0
C	0	0.000033	0.0365	0	0	0

Table 13: MARS15 Material Density

Element	Density (gm/cm^3)
Mg	1.738
Ca	1.55
Conc	2.35
marble	2.7
Ni	8.902
Cr	7.19
Mn	7.33
Mo	10.22
S316	7.92
Cast	7.31
Fe	7.87

Table 14: MARS built-in Isotopic Abundance (Mole Fraction) for Calcium

Isotope	Mole Fraction
Ca-40	0.96941
Ca-42	0.00647
Ca-43	0.00135
Ca-44	0.02086
Ca-46	$4(3) \times 10^{-5}$
Ca-48	0.00187

[5] Igor Rakhno. Radiation shielding for the Main Injector collimation system. TM 2391-AD, Fermilab, 2007.

[6] Bruce C. Brown. Activation of Steel and Copper Samples in the Main Injector Collimator Region. Beams-doc 4046, Fermilab, January 2012.

[7] Bruce C. Brown and Guan Hong Wu. Measuring Correlations Between Beam Loss and Residual Radiation in the Fermilab Main Injector. In Jan Chrin, editor, *Proceedings of the 46th ICFA Advanced Beam Dynamics Workshop on High-Intensity and High-Brightness Hadron Beams (HB2010)*, pages 391–394, Morschach, Switzerland, 2010. Also available as FERMILAB-CONF-10-368-AD.

[8] Management of Main Injector Project. The Fermilab Main Injector Technical Design Handbook. Beams-doc 4294-v1, Fermilab, 1994. Also available from Fermilab Publications Office as FERMILAB-DESIGN-1994-01.

[9] Marcel Barbier. *Induced Radioactivity*. North-Holland Publishing Company, Amsterdam, London, 1969.

[10] Bruce C. Brown, Nikolai V. Mokhov, and Vitaly S. Pronskikh. Activation Products from Copper and Steel Samples Exposed To Showers Produced by 8 GeV Protons Lost at the Fermilab Main Injector Collimation System. In *Proceedings of 12th Workshop on Shielding Aspects of Accelerators, Targets and Irradiation Facilities (SATIF-12) 28 - 30 April 2014 Batavia, Illinois*, 2014.

[11] Pertti A. Aarnio. Decay and Transmutation of Nuclides. CMS-NOTE 1998-086, CERN, January 1999.

[12] Bruce C. Brown. Analysis Procedures for Al Activation Studies. Beams-doc 3980, Fermilab, November 2011.

Table 15: MARS built-in Marble composition

Element	Weight Fraction	Atomic Fraction
Ca	0.400431	0.2
C	0.120005	0.2
O	0.479564	0.6